How to cite: *Angew. Chem. Int. Ed.* **2023**, *62*, e202303574
doi.org/10.1002/anie.202303574

Methane Oxidation

Methane Oxidation over Cu^{2+}/$[CuOH]^+$ Pairs and Site-Specific Kinetics in Copper Mordenite Revealed by Operando Electron Paramagnetic Resonance and UV/Visible Spectroscopy

Jörg Wolfram Anselm Fischer[+], Andreas Brenig[+], Daniel Klose, Jeroen Anton van Bokhoven, Vitaly L. Sushkevich,* and Gunnar Jeschke**

Abstract: Cu-exchanged mordenite (MOR) is a promising material for partial CH_4 oxidation. The structural diversity of Cu species within MOR makes it difficult to identify the active Cu sites and to determine their redox and kinetic properties. In this study, the Cu speciation in Cu-MOR materials with different Cu loadings has been determined using operando electron paramagnetic resonance (EPR) and operando ultraviolet-visible (UV/Vis) spectroscopy as well as in situ photoluminescence (PL) and Fourier-transform infrared (FTIR) spectroscopy. A novel pathway for CH_4 oxidation involving paired $[CuOH]^+$ and bare Cu^{2+} species has been identified. The reduction of bare Cu^{2+} ions facilitated by adjacent $[CuOH]^+$ demonstrates that the frequently reported assumption of redox-inert Cu^{2+} centers does not generally apply. The measured site-specific reaction kinetics show that dimeric Cu species exhibit a faster reaction rate and a higher apparent activation energy than monomeric Cu^{2+} active sites highlighting their difference in the CH_4 oxidation potential.

Introduction

The wasteful handling of natural gas (containing CH_4 as a primary component) in combination with the strive for resource efficiency have strengthened the need for more efficient CH_4 valorization techniques.[1] Current methods start with a steam-reforming step, which is only feasible when conducted at large scale, hence, making the utilization of CH_4 in small quantities from remote sources uneconomical.[2] Therefore, the development of flexible technologies to convert CH_4 on-site into higher-value chemicals is of great interest. One particular approach is the direct oxidation of CH_4 to CH_3OH using Fe- or Cu-exchanged zeolites.[3] In order to improve the selectivity, this reaction is performed in a stoichiometric chemical looping process consisting of material activation, CH_4 oxidation, and product desorption.[3a,4] Among the different zeolites, Cu-containing MOR is considered to be a promising system due to its high density of Cu active sites which results in exceptional CH_3OH yields.[4–5]

Depending on the Si/Al ratio, the local Al distribution, and the Cu content, specific cation exchange positions (site A, B, C, D, and E, Scheme S1) can be populated by Cu^{2+} ions.[6] Cu^{2+} ions incorporated into different exchange sites will experience distinct geometric constraints, which strongly affect their coordination sphere and the possibility to form clusters of different nuclearity.[6f] This leads to multiple Cu^{2+} species that exhibit different redox behavior and activity.[7] At low Cu loading and Si/Al ratio, Cu^{2+} is almost exclusively present as bare, isolated Cu^{2+} ions, balanced by two negative charges on the zeolite.[6a–c,e–g,7b,8] These monomeric Cu^{2+} ions are believed to be inactive in CH_4 oxidation due to the absence of extra-framework O-ligands and due to their low degree of reducibility as a result of their strong electrostatic coordination to the zeolite.[6a–c,f,7b] At least two different types of isolated Cu^{2+} species have been identified using EPR spectroscopy.[6c,e,f] Notwithstanding the proposed chemical inertness of isolated Cu^{2+}, other monomeric transition metal ions incorporated into different zeolites have been proven to participate in CH_4 activation.[9] One example is the conversion of CH_4 on Zn-exchanged Mobil Five (MFI) and Beta (BEA) zeolites into $Zn^{2+}(CH_3)$ and a Brønsted acid site (BAS).[9a,b] These findings raise the question whether bare Cu^{2+} sites are indeed completely inert. With increasing Cu loading, a third monomeric Cu^{2+} species emerges, which occupies cation exchange positions

[*] J. W. A. Fischer,[+] Dr. D. Klose, Prof. Dr. G. Jeschke
Institute for Molecular Physical Science, ETH Zurich
Vladimir-Prelog-Weg 1–5/10, 8093 Zurich (Switzerland)
E-mail: gunnar.jeschke@phys.chem.ethz.ch

A. Brenig,[+] Prof. Dr. J. A. van Bokhoven
Institute for Chemical and Bioengineering, ETH Zurich
Vladimir-Prelog-Weg 1–5/10, 8093 Zurich (Switzerland)
E-mail: jeroen.vanbokhoven@chem.ethz.ch

A. Brenig,[+] Prof. Dr. J. A. van Bokhoven, Dr. V. L. Sushkevich
Laboratory for Catalysis and Sustainable Chemistry, Paul Scherrer Institute
Forschungsstrasse 111, 5232 Villigen (Switzerland)
E-mail: vitaly.sushkevich@psi.ch

[+] co-first authors

characterized by only one Al tetrahedral site (T-site) and, hence, has been ascribed to a $[CuOH]^+$ site.[6a,b,d,e,g,8b,c,10] Due to the weaker interaction with the zeolite lattice these $[CuOH]^+$ centers exhibit a higher reducibility in comparison to bare Cu^{2+}. At high Cu loading, complex Cu-oxo compounds with variable nuclearity, such as dimeric $[Cu_2(\mu\text{-}O)]^{2+}$ species, start to form.[3a,5a,10b,11] These centers occupy less favorable exchange positions and, therefore, feature an even higher degree of reducibility making them especially active in CH_4 oxidation.[6b,d,f,12]

Despite the scientific effort that has been dedicated to the characterization of different Cu^{2+} sites in MOR, their site-specific behavior in CH_4 oxidation requires further assessment. This is illustrated by the fact that the activity of Cu-exchanged zeolites in CH_4 oxidation is typically evaluated on the basis of standardized reactivity tests, which do not distinguish between the activity of individual sites.[13] Therefore, the present study focuses on the analysis of site-specific kinetic properties by employing a time-resolved, multi-spectroscopic approach. The presence and distribution of distinct Cu^{2+} sites in MOR with a Si/Al ratio of 6.5 has been controlled by varying the Cu loading of the prepared materials (Figure S1). Samples are labelled as Cu_xMOR, where x denotes the approximate Cu loading in wt% (Table S1). EPR, UV/Vis, PL, and FTIR spectroscopy have been used to identify different Cu^{2+} species in the ion exchanged samples after a thorough pre-treatment (Figure S2 and S3). Next to $[Cu_2(\mu\text{-}O)]^{2+}$ and proximal $[CuOH]^+$, a comparison of the spectra before and after reaction with CH_4 points towards the participation of bare Cu^{2+} ions in CH_4 conversion. Detailed insight into the kinetic behavior of distinct Cu^{2+} sites has been obtained by operando EPR and UV/Vis spectroscopy, by means of correlating CH_4 consumption with spectroscopic fingerprints. Operando EPR spectroscopy has been used to probe monomeric Cu^{2+} species whereas operando UV/Vis spectroscopy allowed the determination of the reactivity of dimeric $[Cu_2(\mu\text{-}O)]^{2+}$ species. The combination of the site-specific kinetics enables a complete description of the overall CH_4 conversion (Scheme S2).

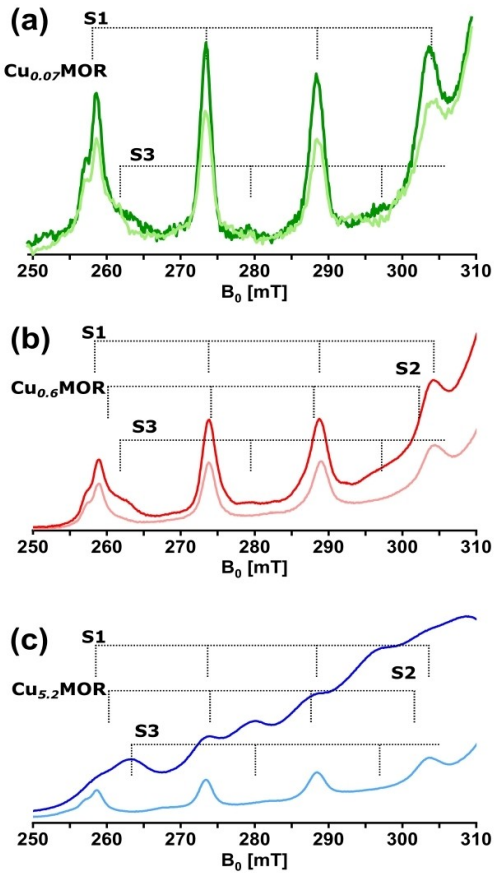

Figure 1. In situ X-band EPR spectra (zoom) recorded at 293 K in vacuum of activated $Cu_{0.07}$MOR (green, (a)), $Cu_{0.6}$MOR (red, (b)), and $Cu_{5.2}$MOR (blue, (c)) as well as the corresponding spectra of $Cu_{0.07}$MOR (light green, (a)), $Cu_{0.6}$MOR (light red, (b)), and $Cu_{5.2}$MOR (light blue. (c)) after the reaction with CH_4 at 473 K. The full spectra recorded at 473 K are shown in Figure S4.

Results and Discussion

The $g_{||}$ splitting region in the EPR spectra of Cu-exchanged zeolites is sensitive towards the geometry and siting of Cu, which enables the differentiation between distinct monomeric Cu^{2+} species.[6c] Cu-oxo centers of higher nuclearity (e.g. $[Cu_2(\mu\text{-}O)]^{2+}$) are considered to be EPR silent due to the antiferromagnetic coupling of O-bridged Cu^{2+} ions.[7b] Spectra of Cu^{2+} feature a characteristic hyperfine quartet of a Cu nucleus ($I=3/2$) interacting with its unpaired electron ($S=1/2$, d^9 configuration).[6c] One-electron reduction of Cu^{2+} results in a closed shell d^{10} configuration causing Cu^+ to be EPR silent, hence, making EPR spectroscopy a sensitive tool to study the reduction of monomeric Cu^{2+} species.[7b] The $g_{||}$ regions of the EPR spectra of the Cu-MOR samples in vacuum before and after the reaction with CH_4 are shown in Figure 1. The spectrum of activated $Cu_{0.07}$MOR is dominated by one Cu^{2+} species, which is also present in the other materials. This species (denoted as site S1, Table 1) features a $g_{||}$ value of 2.32 and has been assigned to a bare Cu^{2+} in an environment with two Al sites arranged in a

Table 1: Distinct spectroscopic signatures of the Cu^{2+} species S1–S4 present in Cu-MOR. Top values correspond to signals identified in this work whereas lower, parenthesized values correspond to features as reported in the literature.

Cu^{2+} species	EPR ($g_{||}$)	UV/Vis [cm^{-1}]	PL [nm]	NO-FTIR [cm^{-1}]
S1	2.32	13000	450	1940
Cu^{2+}	(2.31[6g])	(13700[6b,f])	(450[6g])	(1921[6g,8a])
S2	2.33		480	1940
Cu^{2+}	(2.33[6g])		(480[6g])	(1909[6g,8a])
S3	2.27	–	550	1905
$[CuOH]^+$	(2.27[6g])	(16750[6f])	(540[6g])	(1895[6g,8a])
S4	EPR	26100	–	1954
$[Cu_2(\mu\text{-}O)]^{2+}$	silent (AFC)[7b]	(26100[7b])		(>1940[17])

diagonal fashion.[6g] The presence of an additional species is indicated by a weak shoulder at around 265 mT. The spectrum of activated $Cu_{0.6}$MOR allows to assign this feature to a $[CuOH]^+$ center (denoted as site S3, Table 1) characterized by $g_{||}=2.27$, which is in close proximity to only one Al site.[6h] A third Cu^{2+} species can be identified in $Cu_{0.6}$MOR, which has been attributed to another bare Cu^{2+} site with $g_{||}=2.33$ in an environment with two Al atoms directly across from each other (denoted as site S2, Table 1).[6g] A more detailed description of the assignments is provided by Figure S5–S8. The above mentioned g-tensors and the corresponding A-tensors (Table S2) have been determined at 50 K to enable a comparison with literature results.[14] The same three species, which are present in $Cu_{0.6}$MOR, can also be detected in $Cu_{5.2}$MOR. However, the existence of additional species in $Cu_{5.2}$MOR cannot be excluded, due to the loss in spectral resolution caused by strong Cu^{2+}–Cu^{2+} interactions. A comparison between the spectra of activated and reacted $Cu_{0.6}$MOR and $Cu_{5.2}$MOR reveals that the signal intensity of all three species decreases after CH_4 oxidation indicating their reducibility in the presence of CH_4. In the spectra of all reacted materials, site S1 is the dominant species that remains after the reaction (Figure S5). The small splitting at ~258 mT, which can be observed in each spectrum except the one of activated $Cu_{5.2}$MOR originates from the isotope effect of $^{63/65}$Cu (Figure S5). No Cu-superoxide species were detected by EPR after the activation of the materials (Figure S4).

UV/Vis spectroscopy has been used to investigate Cu^{2+} hosted in Cu-MOR due to their characteristic electronic absorption bands originating from the open d-shell, which gives rise to d-d and ligand-to-metal charge transfer (LMCT) transitions. Figure 2 displays the in situ UV/Vis spectra of the activated Cu-MOR as well as the corresponding spectra after reaction with CH_4. The spectra of all activated materials are characterized by an absorption band (local minimum in reflectance) at ~13000 cm^{-1}, which has been attributed to the d-d transition of sites S1 and S2 (Table 1).[6a–d,f,7b] A rather broad signal at ~36800 cm^{-1} can be observed in the spectra of activated $Cu_{5.2}$MOR and $Cu_{0.6}$MOR, which has been assigned to a LMCT transition from framework O to Cu^{2+}.[6f,10b,11b] In the spectrum of activated $Cu_{5.2}$MOR, another feature at ~26100 cm^{-1} can be observed, which has been associated with the O_{bridge} 2p→Cu^{2+} 3d/4s LMCT transition of dimeric Cu^{2+} species (denoted as site S4, Table 1) such as $[Cu_2(\mu\text{-}O)]^{2+}$ or $[Cu_2(trans\text{-}\mu\text{-}1,2\text{-}O_2)]^{2+}$ centers.[7b,11b,15] Based on X-ray absorption spectroscopy (XAS), Sushkevich et al. attributed this feature to a $[Cu_2(\mu\text{-}O)]^{2+}$ site with a Cu–Cu distance of 2.86 Å.[7b] The presence of trimeric $[Cu_3O_3]^{2+}$ species can be excluded since no pronounced signal at 31000 cm^{-1} can be observed.[13a] Reaction of $Cu_{0.6}$MOR and $Cu_{0.07}$MOR with CH_4 results in the appearance of a new feature centered at ~18500 cm^{-1}, which exhibits a shoulder at about 20200 cm^{-1}. Notably, the reflectance at these positions exceeds the one of the reference indicating PL activity. In fact, monomeric Cu^+ species have been demonstrated to exhibit a PL behavior due to a radiative triplet $3d^9 4s/4p \rightarrow$ singlet $3d^{10}$ transition occurring after excitation.[6b,e,g,8a,c,10a] Therefore, the observation of the features at 18500 and 20200 cm^{-1} suggests that at least two different types of monomeric Cu^{2+} sites have been reduced to Cu^+. This is further highlighted by the loss in absorbance of the band at 13000 cm^{-1} in the spectra of reacted $Cu_{0.6}$MOR and $Cu_{5.2}$MOR. Due to the strong absorption of bands in the d-d region in reflectance mode and the negligible reactivity of $Cu_{0.07}$MOR, this is barely observable in the spectrum of reacted $Cu_{0.07}$MOR.[16] Upon reaction with CH_4, the spectrum of $Cu_{5.2}$MOR is characterized by a drop in absorbance of the band at ~26100 cm^{-1}, which indicates the consumption of the corresponding dimeric site S4.[7b,16] Furthermore, the spectrum of reacted $Cu_{5.2}$MOR shows an increase in the absorbance at ~17770 cm^{-1} that has been associated with adsorbed reac-

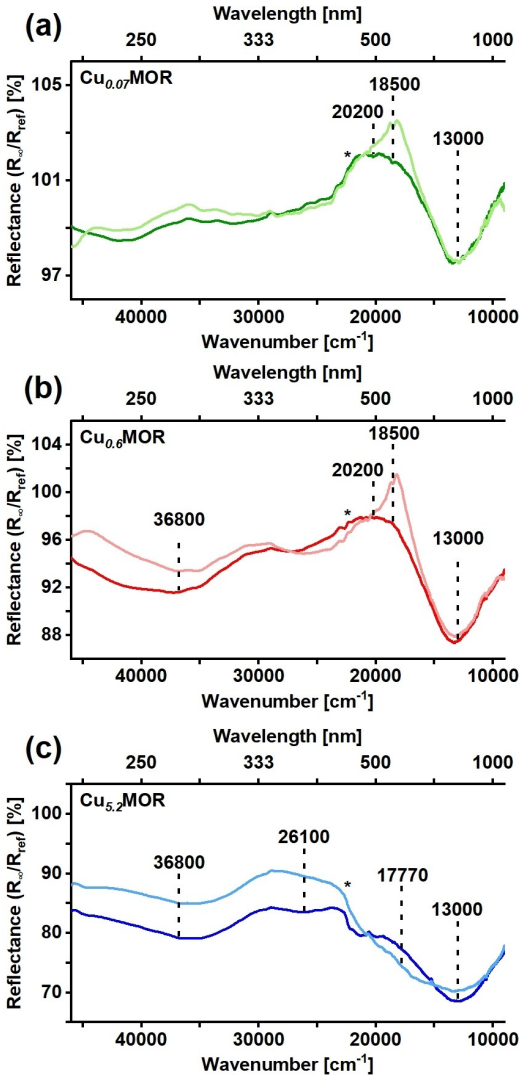

Figure 2. In situ UV/Vis spectra collected at 473 K in vacuum of activated $Cu_{0.07}$MOR (green, (a)), $Cu_{0.6}$MOR (red, (b)), and $Cu_{5.2}$MOR (blue, (c)) as well as the corresponding spectra of $Cu_{0.07}$MOR (light green, (a)), $Cu_{0.6}$MOR (light red, (b)), and $Cu_{5.2}$MOR (light blue, (c)) after the reaction with CH_4 at 473 K. The feature, which is characterized by an inflection point at roughly 22700 cm^{-1} (*), originates from the deuterium/halogen lamp switch.

tion products.[7b] Finally, the spectra of all reacted samples exhibit a loss in absorbance in the region of framework O to Cu^{2+} LMCT transitions suggesting a change in the coordination to the lattice.

PL spectroscopy of Cu^{+} sites in the reacted materials was used to further characterize the PL bands at approximately 20200 and 18500 cm^{-1} observed by UV/Vis spectroscopy. Figure 3 shows the PL spectra of the activated and reacted materials. None of the spectra of the activated materials exhibits a pronounced PL signal, which coincides with the absence of the Cu^{+} 1s→4p edge in the in situ XAS spectra of $Cu_{5.2}$MOR and $Cu_{0.6}$MOR (Figure S10) demonstrating the suitability of the activation procedure. The PL spectra of the reacted $Cu_{5.2}$MOR and $Cu_{0.6}$MOR can be deconvoluted using three Gaussian functions centered at around 450 (~22200 cm^{-1}) 480 (~20800 cm^{-1}), and 550 nm (~18500 cm^{-1}). The signals centered at ~450 and ~480 nm have been assigned to two Cu^{+} centers in different environments initially present as sites S1 and S2 in the activated materials, respectively (Table 1).[6g] The additional PL band at ~550 nm has been associated with a Cu^{+} species, which was previously present as site S3 (Table 1). Compared to $Cu_{0.6}$MOR, the blueshift of the signal at ~550 nm on $Cu_{5.2}$MOR most probably derives from the difference in Cu^{+} speciation due the reduction of the S4 site.[6g] In agreement with both EPR and UV/Vis, the observed PL signals indicate that sites S1 and S2 as well as S3 are getting reduced throughout CH_4 oxidation. The increased PL signal intensity of the features at 450 and 480 nm on $Cu_{5.2}$MOR in comparison to $Cu_{0.6}$MOR indicates a higher degree of reducibility of the S1 and S2 sites at higher Cu loading.

The adsorption of NO on Cu^{2+} and Cu^{+} centers results in a shift of the N–O vibrational frequency, which depends on the Cu speciation and exchange position. As a result, the usage of NO as a probe molecule permits the reliable identification of Cu^{2+} and Cu^{+} via FTIR spectroscopy.[17] Figure 4 displays the FTIR spectra of adsorbed NO of the activated Cu-MOR samples as well as the spectra after reaction with CH_4. The spectra of activated and reacted

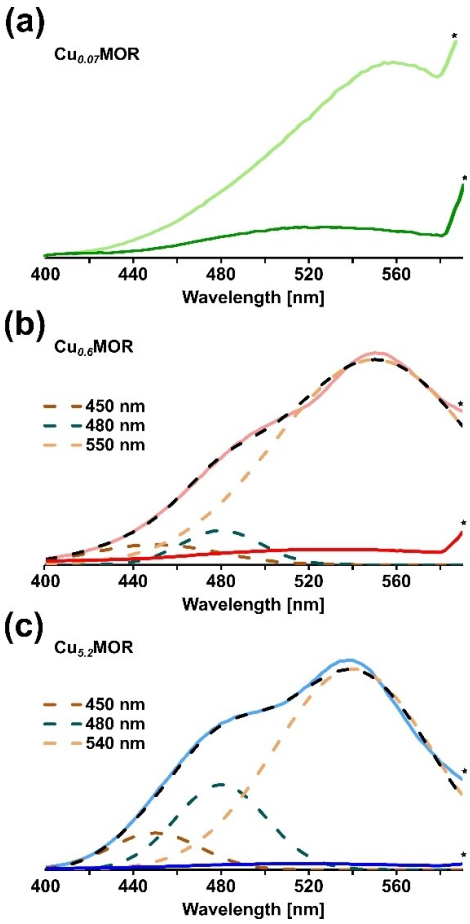

Figure 3. In situ PL spectra recorded at 293 K in vacuum of $Cu_{0.07}$MOR (green, (a)), $Cu_{0.6}$MOR (red, (b)), and $Cu_{5.2}$MOR (blue, (c)) as well as the corresponding spectra of $Cu_{0.07}$MOR (light green, (a)), $Cu_{0.6}$MOR (light red, (b)), and $Cu_{5.2}$MOR (light blue, (c)) after the reaction with CH_4 at 473 K. The low Cu loading in $Cu_{0.07}$MOR in combination with the negligible reactivity of this material prevents a reliable deconvolution. The asterisk (*) marks the beginning second harmonic excitation artifact in the PL spectra. Note that due to the dependency of the ratio of the PL signal intensities on the excitation wavelength, the ratio of the different Cu^{+} species cannot be assessed quantitatively.

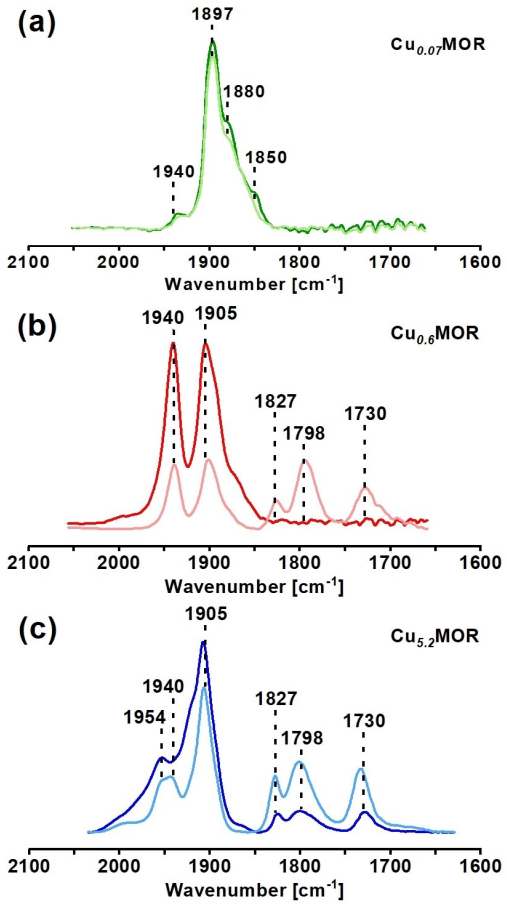

Figure 4. In situ FTIR spectra recorded at 77 K in vacuum of adsorbed NO on activated $Cu_{0.07}$MOR (green, (a)), $Cu_{0.6}$MOR (red, (b)), and $Cu_{5.2}$MOR (blue, (c)) as well as the corresponding spectra of adsorbed NO on $Cu_{0.07}$MOR (light green, (a)), $Cu_{0.6}$MOR (light red, (b)), and $Cu_{5.2}$MOR (light blue, (c)) after the reaction with CH_4 at 473 K.

$Cu_{0.07}$MOR are characterized by signals at ~1897, 1880, and 1850 cm^{-1} as well as a small band at ~1940 cm^{-1}.

The former three signals result from the interaction of NO with the zeolite (Figure S11). Considering the low Cu loading of $Cu_{0.07}$MOR, it is reasonable to assume that the feature at ~1940 cm^{-1} originates from the adsorption of NO on sites S1 and S2 (Table 1). Apart from the signal at ~1940 cm^{-1}, the spectrum of activated $Cu_{0.6}$MOR exhibits an additional feature at ~1905 cm^{-1}. Based on the higher Cu loading of this sample, this band could be associated with the adsorption of NO on site S3 (Table 1). Similar results regarding the assignment of these features were reported by Palagin et al..[17] The spectra of activated and reacted $Cu_{5.2}$MOR are characterized by an additional band at ~1954 cm^{-1}. This feature has been attributed to the interaction of NO with aggregated Cu^{2+} sites.[7b,c] Since $Cu_{5.2}$MOR exhibits the electronic absorption band at ~26100 cm^{-1} corresponding to the dimeric site S4 (Figure 2), it can be suggested that the signal at 1954 cm^{-1} originates from a $[Cu_2(\mu\text{-}O)]^{2+}(NO)$ complex (Table 1). The spectrum of reacted $Cu_{0.6}$MOR as well as the spectra of activated and reacted $Cu_{5.2}$MOR display bands at ~1827, 1798, and 1730 cm^{-1} that correspond to NO adsorbed on Cu^{+}.[6g,8c] These features cannot be detected on $Cu_{0.07}$MOR due to the low Cu loading and marginal reactivity in combination with the lower sensitivity of NO-FTIR. The feature at ~1798 cm^{-1} has been associated with a $Cu^{+}(NO)$ mononitrosyl complex, whereas the signals at 1827 and 1730 cm^{-1} have been attributed to the symmetric and antisymmetric stretching frequencies of $Cu^{+}(NO)_2$ dinitrosyl complexes, respectively. The appearance of these bands in the spectrum of activated $Cu_{5.2}$MOR suggests a small degree of autoreduction throughout the experimental procedure. The loss in absorbance of the signals at ~1954, 1940, and 1905 cm^{-1} in the spectra of reacted $Cu_{0.6}$MOR and $Cu_{5.2}$MOR further emphasizes the reduction of sites S1–S4 during CH_4 oxidation.

The site-specific reaction kinetics of monomeric Cu^{2+} species (sites S1–S3) have been determined by following the decrease of the Cu^{2+} signals during CH_4 oxidation with time-resolved EPR spectroscopy. In addition, since CH_4 does not adsorb on the pure zeolite surface (Figure S19) at the employed reaction temperatures, the simultaneously recorded CH_4 pressure is equivalent to the reactant concentration. Hence, following the decay in CH_4 pressure allows to assess the performance of all Cu^{2+} sites active in CH_4 oxidation. Figure 5a illustrates an exemplary series of EPR spectra acquired during the reaction of $Cu_{5.2}$MOR with CH_4 at 473 K. The full set of operando EPR spectra is shown in Figure S12. In addition, Figure 5b displays the temporal evolution of the double integral intensity of $Cu_{5.2}$MOR at four different reaction temperatures (Figure S13) as well as the simultaneously recorded CH_4 pressure (Figure 5c). The development of the double integral intensity of $Cu_{0.6}$MOR at the same temperatures as well as the corresponding CH_4 pressure are shown in Figure S14. As a result of the negligible activity of $Cu_{0.07}$MOR, no pronounced decrease in EPR signal intensity can be detected (Figure 1). On the contrary, the reduction of Cu^{2+} in $Cu_{0.6}$MOR and $Cu_{5.2}$MOR is clearly observable in the EPR spectra (Figure 1) and their reaction rate constants can be determined from the decay of the double integral intensity. The latter was described by a sum of a first-order reaction rate law and a linear function (Table S5 and S7) to account for the quasi-linear regime after 7000 s. The additional kinetic contribution by this linear term is, however, unrelated to CH_4 oxidation (Figure S16). Based on the first-order reaction rate component, the reaction rate constants were derived and the resulting Arrhenius plot is shown in Figure 5d. $Cu_{0.6}$MOR and $Cu_{5.2}$MOR are characterized by apparent activation energies of 36 and 35 kJ/mol, respectively. The reaction rate constants of $Cu_{5.2}$MOR are approximately four times higher than the ones of $Cu_{0.6}$MOR due to the higher Cu loading of the former.[7b] Since the total CH_4 consumption is a result of both monomeric (S1–S3) and dimeric (S4) Cu^{2+} species, which exhibit different kinetic behaviors, the decrease in CH_4 pressure on $Cu_{5.2}$MOR has been described by a sum of two first-order reaction rate laws (Table S6) assuming that the reaction is pseudo zero order with respect to CH_4.[7b] The statistical relevance of the model parameters is evaluated in Table S11.

$$A(t) = A_{S1-S3}^{CH_4} * e^{-k_{S1-S3}^{CH_4} * t} + A_{S4}^{CH_4} * e^{-k_{S4}^{CH_4} * t}$$

Here A(t) denotes the time-dependent amount of all Cu^{2+} active sites, $A_{S1-S3}^{CH_4}$ and $A_{S4}^{CH_4}$ describe the initial amount of monomeric and dimeric active sites, respectively, and $k_{S1-S3}^{CH_4}$ and $k_{S4}^{CH_4}$ correspond to their reaction rate constants. Applying this model to the recorded CH_4 pressure yields the reaction rate constants of both monomeric and dimeric Cu^{2+} sites, which were subsequently used to determine their apparent activation energies (Figure 5d). The apparent activation energy of monomeric Cu^{2+} centers was found to be 38 kJ/mol, which is in agreement with the results of the recorded EPR spectra. An apparent activation energy of 66 kJ/mol was determined for dimeric Cu^{2+} centers.

The kinetic behavior of dimeric Cu^{2+} species (site S4) as well as the total CH_4 conversion were further studied by means of operando UV/Vis spectroscopy. Figure 6a displays an illustrative set of difference spectra of $Cu_{5.2}$MOR recorded throughout CH_4 oxidation at 473 K. The full set of operando UV/Vis spectra is shown in Figure S17. The changes in the integrated intensity of the signal at ~26100 cm^{-1} at the same temperatures as in the operando EPR experiments are also shown Figure 6b in addition to the simultaneously recorded CH_4 pressure (Figure 6c). The measured CH_4 pressure on $Cu_{0.07}$MOR and $Cu_{0.6}$MOR are shown in Figure S19. As Figure 6a illustrates, the decay in integrated intensity of the band at ~26100 cm^{-1} in $Cu_{5.2}$MOR can be described by a first-order reaction rate equation (Table S9). On the basis of the identified reaction rate constants, the apparent activation energy was determined to be 60 kJ/mol (Figure 6d). As mentioned above, the CH_4 pressure during CH_4 oxidation on $Cu_{5.2}$MOR can be described by a sum of two first-order reaction rate laws (Table S10). On the contrary, the CH_4 pressure during the reaction of $Cu_{0.6}$MOR with CH_4 was fitted by a first-order

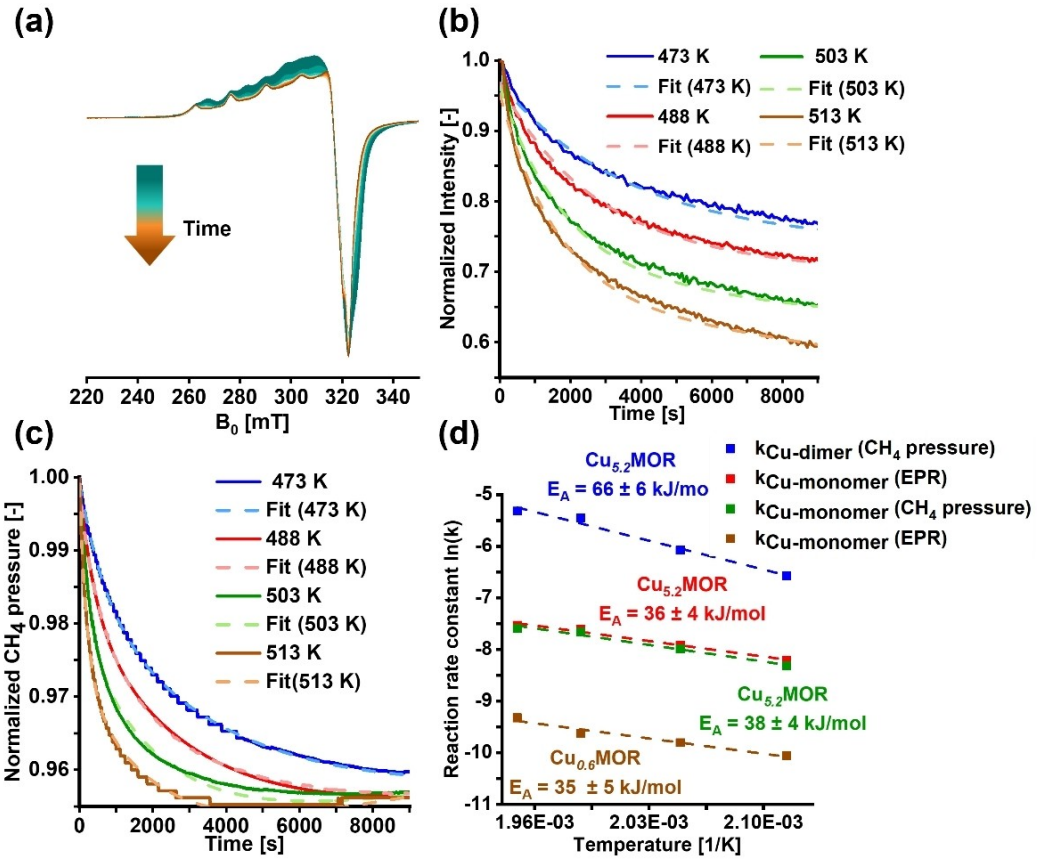

Figure 5. Series of EPR spectra of $Cu_{5.2}$MOR recorded during CH_4 oxidation at 473 K (a), the normalized double integral intensity of the EPR spectra of $Cu_{5.2}$MOR at reaction temperatures in the range from 473 to 513 K (b), normalized CH_4 pressure on $Cu_{5.2}$MOR (c), and the Arrhenius plots based on reaction rate constants obtained from either the double integral intensity of the EPR spectra of $Cu_{5.2}$MOR and $Cu_{0.6}$MOR or the normalized CH_4 pressure on $Cu_{5.2}$MOR during CH_4 oxidation (d).

reaction rate law as only monomeric Cu^{2+} species are present in this sample (Table S12). The apparent activation energy of dimeric Cu^{2+} species in $Cu_{5.2}$MOR accounts for 60 kJ/mol whereas the apparent activation energies of monomeric Cu^{2+} sites in $Cu_{0.6}$MOR and $Cu_{5.2}$MOR are 28 and 35 kJ/mol, respectively. The apparent activation energy of dimeric Cu^{2+} sites as determined from either the loss in the integrated intensity or the decay in CH_4 pressure are in good agreement with each other.

Three Cu-MOR samples with different Cu loadings have been synthesized and their performance in CH_4 oxidation has been assessed (Table S13). The Cu speciation has been studied by a time-resolved multi-spectroscopic approach allowing the identification and kinetic characterization of Cu^{2+} species. The kinetic properties of the present Cu^{2+} active sites can be used to fully describe the total CH_4 consumption during operando experiments. Depending on the Cu loading, four different types of Cu^{2+} centers have been identified, including two types of bare Cu^{2+} ions (sites S1 and S2), $[CuOH]^+$ (site S3), and $[Cu_2(\mu\text{-}O)]^{2+}$ (site S4) species (Table 1).

A combination of EPR spectroscopy and theoretical calculations has indicated that bare Cu^{2+} ions are located within the planar 6-mebered ring (MR) of site E where they adopt a distorted, fourfold coordination.[5a,6a,c,e] Since the Al T-sites can either be placed directly across from each other or in a diagonal manner, two types of isolated Cu^{2+} ions corresponding to sites S1 and S2, respectively, can be formed.[6c,e,f] Theoretical calculations have indicated that the 12-MR as well as the planar 6-MR of site E and the planar 5-MR of site C characterized by Al at different T-sites can host site S3.[5a,6a,c,7b,c] Since these centers are in proximity to only one Al T-site, an extra-lattice OH^- ligand has been suggested to account for charge compensation.[6a,c,7b,8b,c,10a]

Due to the energetically favorable fourfold coordination and strong interaction with the MOR lattice, site S1 is present in all prepared materials.[6a,f] This is shown by the fact that all EPR spectra of the activated materials exhibit features with a $g_{||}$ value of 2.32 (Table 1). Additionally, site S2 characterized by a $g_{||}$ value of 2.33 can be identified in $Cu_{0.6}$MOR and $Cu_{5.2}$MOR. All UV/Vis spectra as well as the FTIR spectra of adsorbed NO feature the corresponding absorption bands at ~13000 cm^{-1} and ~1940 cm^{-1}, respectively. Further support is given by the observed Cu^+ PL bands centered at around 450 and 480 nm in the PL spectra of reacted $Cu_{0.6}$MOR and $Cu_{5.2}$MOR. The decrease in signal

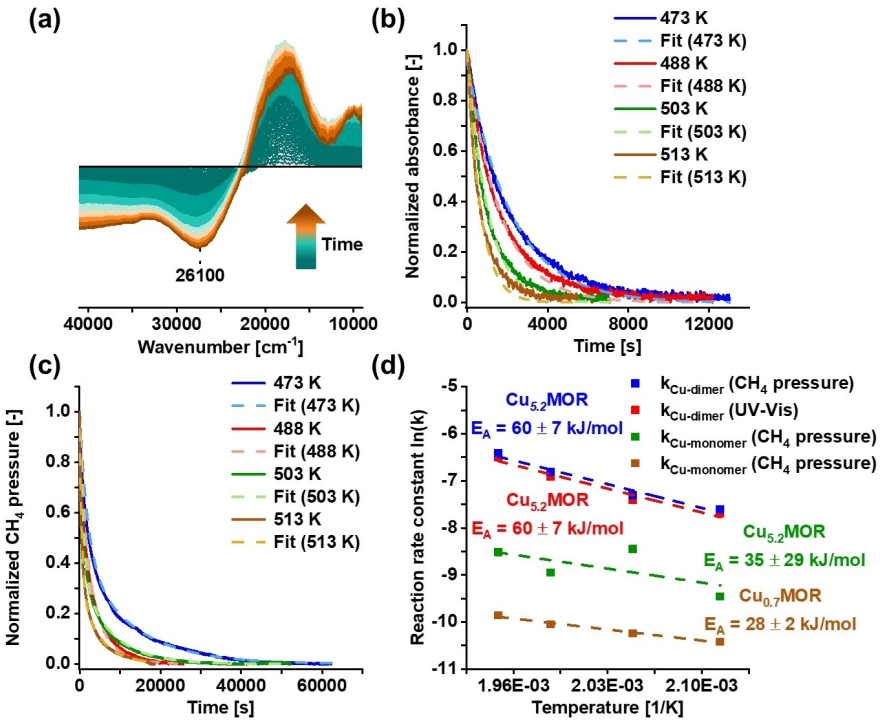

Figure 6. Series of difference spectra of $Cu_{5.2}$MOR recorded during CH_4 oxidation at 473 K (a), normalized absorbance of the band at ~26100 cm^{-1} in UV/Vis spectra of $Cu_{5.2}$MOR at reaction temperatures in the range from 473 to 513 K (b), normalized CH_4 pressure on $Cu_{5.2}$MOR (c), and the Arrhenius plots based on reaction rate constants obtained from either the normalized absorbance of the signal at ~26100 cm^{-1} in UV/Vis spectra of $Cu_{5.2}$MOR or the normalized CH_4 pressure on $Cu_{5.2}$MOR and $Cu_{0.6}$MOR during CH_4 oxidation (d).

intensity of the spectroscopic features of sites S1 and S2 in the EPR, UV/Vis, and FTIR spectra of $Cu_{5.2}$MOR and $Cu_{0.6}$MOR upon reaction with CH_4 as well as the concomitant appearance of the Cu^+ PL bands in the UV/Vis and PL spectra clearly demonstrate the participation of these species in CH_4 oxidation. A simple thermally induced reduction of sites S1 and S2 by CH_4 can be excluded since such a process requires reaction temperatures well above 623 K.[18] Furthermore, sites S1 and S2 as well as S3 are all accessible via the main 12-MR channel, hence, allowing their interaction with CH_4.[6a–c]

Upon increase in Cu loading, site S3 becomes more visible, as evident by the emerging feature with a $g_{||}$ value of 2.27 in EPR spectra and the band at ~1905 cm^{-1} in FTIR spectra of adsorbed NO of $Cu_{0.6}$MOR (Table 1). In contrast to the results of Vanelderen et al., no distinct absorption signal at 16750 cm^{-1} in the UV/Vis spectra corresponding to the d-d transition in site S3 could be detected.[6f] However, this does not exclude the presence of these Cu^{2+} species since the spectral region of d-d transitions in Cu-MOR has been reported to suffer from low resolution as a result of vibronic broadening.[4] Furthermore, the UV/Vis spectra of reacted $Cu_{0.07}$MOR and $Cu_{0.6}$MOR as well as the PL spectra of reacted $Cu_{5.2}$MOR and $Cu_{0.6}$MOR exhibit a Cu^+ PL signal centered at ~550 nm clearly indicating the presence of site S3. The reduction of site S3 during CH_4 oxidation is shown by the decrease of the corresponding EPR signal, the loss of the band in FTIR spectra of adsorbed NO at 1905 cm^{-1}, and the appearance of the Cu^+ PL signal at ~550 nm in UV/Vis and PL spectra.

The reactivity of paired $[CuOH]^+$ towards CH_4 in MOR as well as in other frameworks has been reported.[7b,c,19] Nevertheless, the observed participation of sites S1 and S2 during CH_4 oxidation is remarkable because these species have been considered to be chemically inert in most literature reports as a result of their low reducibility.[6a–c,f] In addition, they are not coordinated to extra-framework O atoms which are required for the CH_4 to CH_3OH conversion. Because H_2O or NO_x can be excluded as a relevant source of O atoms due to the extensive pre-treatment (Figure S3), it can be suggested that an additional Cu-oxo species in close proximity facilitates their reduction. Considering that sites S1 and S2 in $Cu_{0.6}$MOR and a marginal amount of S1 in $Cu_{0.07}$MOR are reduced even though they do not contain S4 centers, the possible source of extra-framework O is suggested to be site S3. In addition, EPR spectra of all reacted materials show that site S1 is the dominant species remaining after CH_4 oxidation, implying that Cu^{2+} cannot be reduced without proximate Cu-oxo species. Since a dynamic interconversion of Cu^{2+} centers is not expected as a result of the irrelevant amount of mobilizing groups, a possible reaction pathway involving the reduction of a $Cu^{2+}/[CuOH]^+$ pair and the consecutive formation of a BAS upon CH_4 oxidation is proposed (Scheme 1).[20]

The generation of BAS during CH_4 oxidation on (S1–S2)/S3 pairs is evident from the increase in signal intensity

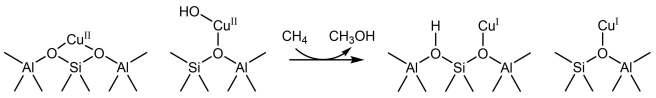

Scheme 1. Proposed CH_4 oxidation pathway on proximate Cu^{2+}/$[CuOH]^+$ pairs.

of a band at 3629 cm^{-1} in the FTIR spectrum of reacted $Cu_{0.6}$MOR (Figure S20). Such a high-frequency O–H vibration has been associated with BAS located in the 6-MR of site E which has also been suggested to host bare Cu^{2+} ions.[5a,6c,21] and is therefore in agreement with the proposed mechanism. BAS formation via CH_4 oxidation on dimeric S4 centers can be neglected in this case since $Cu_{0.6}$MOR does not contain aggregated Cu^{2+} species due to its low Cu loading. Furthermore, a contribution to the BAS signal intensity from overoxidized reaction products can be excluded since these species are not detectable on $Cu_{0.6}$MOR (Figure S21). Interestingly, bare Cu^{2+} species in Cu-exchanged MFI have recently been suggested to be involved in the C–H bond activation of the CH_4 molecule.[22]

At last, site S4 is only present in $Cu_{5.2}$MOR due to its high Cu loading. This is demonstrated by the absorption band at ~26100 cm^{-1} in the UV/Vis spectrum as well as the feature at ~1945 cm^{-1} in the FTIR spectrum of adsorbed NO (Table 1). Based on the changes observed in the UV/Vis and FTIR spectra, site S4 seems to exhibit a pronounced activity, which is in accordance with earlier results.[7b,23] Several reports have demonstrated the existence of two different types of $[Cu_2(\mu\text{-}O)]^{2+}$ located in either site B or stretched across two opposing 8-MR windows of site D, which differ in terms of their kinetic behavior in CH_4 oxidation.[5a,11a] Since the loss of the integrated intensity of the UV/Vis band of site S4 is, however, described best by a single exponential decay no evidence for the presence of two different dimeric species can be found. Compared to monomeric centers, site S4 is prone to autoreduction, which is evident from the resulting bands of $Cu^+(NO)_x$ complexes in the FTIR spectrum of absorbed NO of activated $Cu_{5.2}$MOR. In addition, $Cu_{5.2}$MOR is characterized by a considerably lower CH_3OH selectivity as highlighted by the more pronounced signal intensity of features originating from overoxidized reaction products in the corresponding FTIR spectra after CH_4 oxidation (Figure S21). This is in agreement with the larger amount of CO_2 detected during product desorption in reactivity tests (Table S13). A summary of the distinct spectroscopic features of sites S1–S4 as well as their activity in CH_4 to CH_3OH conversion is illustrated in Scheme 2.

The apparent activation energies of sites S1–S3 in $Cu_{0.6}$MOR and $Cu_{5.2}$MOR derived from operando EPR spectroscopy are similar and indicate that CH_4 oxidation proceeds via the same reaction pathways in both materials. Based on the simultaneously recorded decrease in CH_4 pressure on $Cu_{5.2}$MOR, the apparent activation energy of site S4 has been determined by operando EPR spectroscopy and the results are in high agreement with those obtained by complementary operando UV/Vis spectroscopy experiments. Furthermore, the apparent activation energies of sites S1–S3 deduced from the CH_4 consumption in operando UV/Vis experiments on $Cu_{0.6}$MOR and $Cu_{5.2}$MOR are well in line with the results of operando EPR spectroscopy experiments. In both operando EPR and UV/Vis spectroscopy experiments, the reaction rate constants of site S4 are significantly higher in comparison to the ones of sites S1–S3. The noticeably faster reaction rate constants of site S4 are well in line with their pronounced reducibility and high activity in CH_4 oxidation.[6b,d,f,12]

Conclusion

A novel reaction pathway over Cu^{2+}/$[CuOH]^+$ pairs has been identified and a reaction mechanism involving Brønsted acid site formation has been suggested. The site-specific reaction kinetics and apparent activation energies of combined monomeric and dimeric Cu^{2+} species have been determined using operando EPR and operando UV/Vis spectroscopy. The results of both spectroscopy techniques

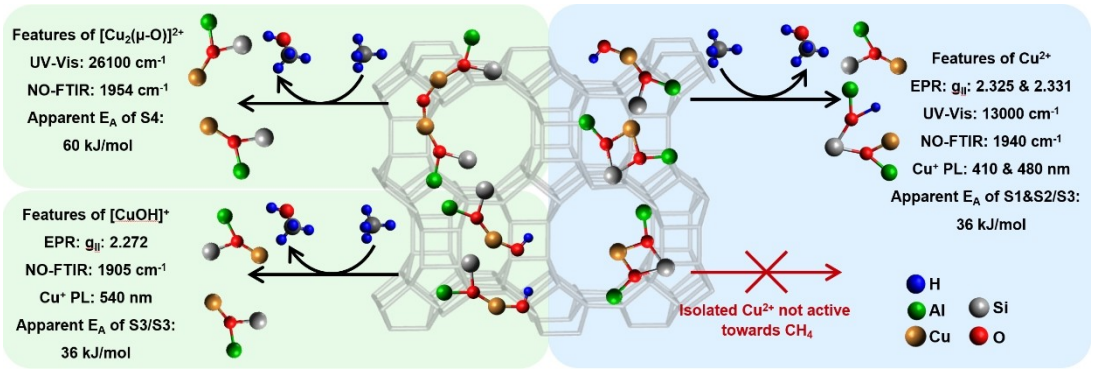

Scheme 2. Compilation of different Cu species in Cu-MOR, their characteristic spectroscopic fingerprints as well as specific reaction pathways in direct CH_4 to CH_3OH oxidation and their corresponding activation energies. Isolated Cu^{2+} species that are not in close proximity to another Cu site bearing extra-framework oxygen are not active towards CH_4. Pathways shown in green are literature known, whereas the novel pathway is highlighted in blue.

are in good agreement with each other and reveal that the total CH_4 conversion can be fully described by the sum of the kinetic contributions from both monomeric and dimeric Cu^{2+} active sites. The combination of the two techniques enables an in-depth analysis of the activity of all present Cu^{2+} sites that would not have been possible by standardized reactivity tests. As a result, the findings of the present study comprehensively elucidate the structure-performance relationship of Cu^{2+} sites in Cu-exchanged MOR and improve the understanding of material behavior in CH_4 to CH_3OH conversion.

Acknowledgements

Funding for this work was provided by the ETH Research Grant ETH-48 20-1 as well as the Energy System Integration (ESI) platform of the Paul Scherrer Institute. We gratefully acknowledge the support from René Tschaggelar and Oliver Oberhänsli in the development of the operando EPR setup as well as the Swiss Light Source (SLS) of the Paul Scherrer Institute for providing beamtime access at the SuperXAS beam line. We thank Prof. Dr. Maksym Kovalenko for the access to the PL spectrometer. We also thank Daniel Zindel for the analysis of the $Cu(pic)_2$:$Zn(pic)_2$ reference. We thank the anonymous reviewer for the suggestion to perform CH_4 partial oxidation in the presence of H_2O. Open Access funding provided by Eidgenössische Technische Hochschule Zürich.

Conflict of Interest

The authors declare no conflict of interest.

Data Availability Statement

The data that support the findings of this study are available from the corresponding author upon reasonable request.

Keywords: Copper · heterogeneous catalysis · methane to methanol · operando spectroscopy · zeolites

[1] M. H. Mahyuddin, Y. Shiota, K. Yoshizawa, *Catal. Sci. Technol.* **2019**, *9*, 1744–1768.

[2] a) M. Ravi, M. Ranocchiari, J. A. van Bokhoven, *Angew. Chem. Int. Ed.* **2017**, *56*, 16464–16483; b) Z. R. Jovanovic, J. P. Lange, M. Ravi, A. J. Knorpp, V. L. Sushkevich, M. A. Newton, D. Palagin, J. A. van Bokhoven, *J. Catal.* **2020**, *385*, 238–245.

[3] a) M. H. Groothaert, P. J. Smeets, B. F. Sels, P. A. Jacobs, R. A. Schoonheydt, *J. Am. Chem. Soc.* **2005**, *127*, 1394–1395; b) E. V. Starokon, M. V. Parfenov, S. S. Arzumanov, L. V. Pirutko, A. G. Stepanov, G. I. Panov, *J. Catal.* **2013**, *300*, 47–54.

[4] M. A. Newton, A. J. Knorpp, V. L. Sushkevich, D. Palagin, J. A. van Bokhoven, *Chem. Soc. Rev.* **2020**, *49*, 1449–1486.

[5] a) P. Vanelderen, B. E. R. Snyder, M. L. Tsai, R. G. Hadt, J. Vancauwenbergh, O. Coussens, R. A. Schoonheydt, B. F. Sels, E. I. Solomon, *J. Am. Chem. Soc.* **2015**, *137*, 6383–6392; b) I. Lee, M. S. Lee, L. Tao, T. Ikuno, R. Khare, A. Jentys, T. Huthwelker, C. N. Borca, A. Kalinko, O. Y. Gutierrez, N. Govind, J. L. Fulton, J. Z. Hu, V. A. Glezakou, R. Rousseau, M. Sanchez-Sanchez, J. A. Lercher, *JACS Au* **2021**, *1*, 1412–1421; c) T. Ikuno, S. Grundner, A. Jentys, G. N. Li, E. Pidko, J. Fulton, M. Sanchez-Sanchez, J. A. Lercher, *J. Phys. Chem. C* **2019**, *123*, 8759–8769.

[6] a) A. Delabie, K. Pierloot, M. H. Groothaert, R. A. Schoonheydt, L. G. Vanquickenborne, *Eur. J. Inorg. Chem.* **2002**, *2002*, 515–530; b) P. Vanelderen, J. Vancauwenbergh, B. F. Sels, R. A. Schoonheydt, *Coord. Chem. Rev.* **2013**, *257*, 483–494; c) A. Delabie, K. Pierloot, M. H. Groothaert, B. M. Weckhuysen, R. A. Schoonheydt, *Phys. Chem. Chem. Phys.* **2002**, *4*, 134–145; d) P. J. Smeets, J. S. Woertink, B. F. Sels, E. I. Solomon, R. A. Schoonheydt, *Inorg. Chem.* **2010**, *49*, 3573–3583; e) J. Dedecek, B. Wichterlova, *Phys. Chem. Chem. Phys.* **1999**, *1*, 629–637; f) P. Vanelderen, J. Vancauwenbergh, R. G. Hadt, M. L. Tsai, B. E. R. Snyder, E. I. Solomon, R. A. Schoonheydt, B. F. Sels, *ChemPhysChem* **2014**, *15*, 91–99; g) J. Dedecek, Z. Sobalik, Z. Tvaruzkova, D. Kaucky, B. Wichterlova, *J. Phys. Chem.* **1995**, *99*, 16327–16337; h) A. J. Heyer, D. Plessers, A. Braun, H. M. Rhoda, M. L. Bols, B. Hedman, K. O. Hodgson, R. A. Schoonheydt, B. F. Sels, E. I. Solomon, *J. Am. Chem. Soc.* **2022**, *144*, 19305–19316.

[7] a) V. L. Sushkevich, R. Verel, J. A. van Bokhoven, *Angew. Chem. Int. Ed.* **2020**, *59*, 910–918; b) V. L. Sushkevich, M. Artsiusheuski, D. Klose, G. Jeschke, J. A. van Bokhoven, *Angew. Chem. Int. Ed.* **2021**, *60*, 15944–15953; c) V. L. Sushkevich, D. Palagin, J. A. van Bokhoven, *Angew. Chem. Int. Ed.* **2018**, *57*, 8906–8910.

[8] a) B. Wichterlova, J. Dedecek, Z. Sobalik, A. Vondrova, K. Klier, *J. Catal.* **1997**, *169*, 194–202; b) J. Dedecek, B. Wichterlova, *J. Phys. Chem.* **1994**, *98*, 5721–5727; c) B. Wichterlova, Z. Sobalik, J. Dedecek, *Catal. Today* **1997**, *38*, 199–203.

[9] a) A. A. Gabrienko, S. S. Arzumanov, M. V. Luzgin, A. G. Stepanov, V. N. Parmon, *J. Phys. Chem. C* **2015**, *119*, 24910–24918; b) A. A. Gabrienko, S. S. Arzumanov, A. V. Toktarev, I. G. Danilova, I. P. Prosvirin, V. V. Kriventsov, V. I. Zaikovskii, D. Freude, A. G. Stepanov, *ACS Catal.* **2017**, *7*, 1818–1830; c) A. A. Gabrienko, S. S. Arzumanov, I. B. Moroz, A. V. Toktarev, W. Wang, A. G. Stepanov, *J. Phys. Chem. C* **2013**, *117*, 7690–7702; d) Y. G. Kolyagin, I. I. Ivanova, V. V. Ordomsky, A. Gedeon, Y. A. Pirogov, *J. Phys. Chem. C* **2008**, *112*, 20065–20069.

[10] a) B. Wichterlova, Z. Sobalik, A. Vondrova, *Catal. Today* **1996**, *29*, 149–153; b) P. J. Smeets, M. H. Groothaert, R. A. Schoonheydt, *Catal. Today* **2005**, *110*, 303–309.

[11] a) B. E. R. Snyder, P. Vanelderen, R. A. Schoonheydt, B. F. Sels, E. I. Solomon, *J. Am. Chem. Soc.* **2018**, *140*, 9236–9243; b) G. Brezicki, J. Zheng, C. Paolucci, R. Schlogl, R. J. Davis, *ACS Catal.* **2021**, *11*, 4973–4987.

[12] D. Palagin, A. J. Knorpp, A. B. Pinar, M. Ranocchiari, J. A. van Bokhoven, *Nanoscale* **2017**, *9*, 1144–1153.

[13] a) S. Grundner, W. Luo, M. Sanchez-Sanchez, J. A. Lercher, *Chem. Commun.* **2016**, *52*, 2553–2556; b) J. Zheng, I. Lee, E. Khramenkova, M. Wang, B. Peng, O. Y. Gutierrez, J. L. Fulton, D. M. Camaioni, R. Khare, A. Jentys, G. L. Haller, E. A. Pidko, M. Sanchez-Sanchez, J. A. Lercher, *Eur. J. Chem.* **2020**, *26*, 7515–7515; c) M. A. Artsiusheuski, R. Verel, J. A. van Bokhoven, V. L. Sushkevich, *ACS Catal.* **2021**, *11*, 12543–12556.

[14] A. Godiksen, P. N. R. Vennestrøm, S. B. Rasmussen, S. Mossin, *Top. Catal.* **2017**, *60*, 13–29.

[15] O. Adeyiga, O. Suleiman, S. O. Odoh, *Inorg. Chem.* **2021**, *60*, 8489–8499.
[16] C. Negri, M. Signorile, N. G. Porcaro, E. Borfecchia, G. Berlier, T. V. W. Janssens, S. Bordiga, *Appl. Catal. A* **2019**, *578*, 1–9.
[17] D. Palagin, V. L. Sushkevich, A. J. Knorpp, M. Ranocchiari, J. A. van Bokhoven, *J. Phys. Chem. C* **2021**, *125*, 12094–12106.
[18] S. C. M. Mizuno, S. Dulnee, T. C. P. Pereira, R. J. Passini, E. A. Urquieta-Gonzalez, J. M. R. Gallo, J. B. O. Santos, J. M. C. Bueno, *Catal. Today* **2021**, *381*, 13–25.
[19] A. J. Knorpp, A. B. Pinar, C. Baerlocher, L. B. McCusker, N. Casati, M. A. Newton, S. Checchia, J. Meyet, D. Palagin, J. A. van Bokhoven, *Angew. Chem. Int. Ed.* **2021**, *60*, 5854–5858.
[20] K. T. Dinh, M. M. Sullivan, K. Narsimhan, P. Serna, R. J. Meyer, M. Dincă, Y. Román-Leshkov, *J. Am. Chem. Soc.* **2019**, *141*, 11641–11650.
[21] D. B. Lukyanov, T. Vazhnova, N. Cherkasov, J. L. Casci, J. J. Birtill, *J. Phys. Chem. C* **2014**, *118*, 23918–23929.
[22] A. A. Gabrienko, S. A. Yashnik, A. A. Kolganov, A. M. Sheveleva, S. S. Arzumanov, M. V. Fedin, F. Tuna, A. G. Stepanov, *Inorg. Chem.* **2020**, *59*, 2037–2050.
[23] J. S. Woertink, P. J. Smeets, M. H. Groothaert, M. A. Vance, B. F. Sels, R. A. Schoonheydt, E. I. Solomon, *PNAS* **2009**, *106*, 18908–18913.

Manuscript received: March 10, 2023
Accepted manuscript online: June 9, 2023
Version of record online: July 11, 2023